



EUMETSAT/ECMWF Fellowship Programme
Research Report No. 39

Scene-dependent observation errors for the assimilation of AMSU-A

Heather Lawrence, Niels Bormann and Stephen
English

August 2015

Series: EUMETSAT/ECMWF Fellowship Programme Research Reports

A full list of ECMWF Publications can be found on our web site under:

<http://www.ecmwf.int/en/research/publications>

Contact: library@ecmwf.int

©Copyright 2015

European Centre for Medium Range Weather Forecasts
Shinfield Park, Reading, RG2 9AX, England

Literary and scientific copyrights belong to ECMWF and are reserved in all countries. This publication is not to be reprinted or translated in whole or in part without the written permission of the Director-General. Appropriate non-commercial use will normally be granted under the condition that reference is made to ECMWF.

The information within this publication is given in good faith and considered to be true, but ECMWF accepts no liability for error, omission and for loss or damage arising from its use.

Abstract

In this report we present work done to develop new observation errors for the AMSU-A instrument in the ECMWF Numerical Weather Prediction (NWP) system. The new observation errors combine a constant term for channels 5 - 14 with forward model error terms for cloud and surface-sensitive channels (channels 5 - 8). Different constant terms are used for each satellite instrument for channels 5 - 13, in order to account for different instrument noise values. The forward model errors include an emissivity error term, which is based on a simplified physical equation, and a liquid water cloud term over ocean to account for cloud-detection errors, which is an empirical equation derived from background departures. We present here the derivation of the new observation errors and results of assimilation trials to test their impact on forecast quality. The new observation errors were found to have a neutral impact on forecast scores when used with operational quality control with a small positive impact on the short-range forecast fits to ATMS observations, indicating an improved short-range forecast. To further test the new observation errors assimilation trials with relaxed cloud and orography screening were run, allowing the assimilation of more data with more variation in observation errors. This produced mixed results. Relaxing the orography screening led to a neutral impact except over Antarctica where some negative impacts were observed. The relaxed cloud screening improved fits of short-range forecasts to ATMS channels 6 - 7 and had a mainly neutral impact on forecast scores with the exception of some localised degradations over the Southern Hemisphere short-range temperature forecasts at 1000 hPa, diagnosed to be due to the new channel 5 data. The degradations over Antarctica and the Southern Hemisphere ocean are likely due to the introduction of biased data. When relaxing the cloud screening for channels 6 - 8, forecast scores were neutral and a small improvement in the fits of short-range forecasts to ATMS channel 7 was observed. Given results of these trials, the new observation errors were combined with a relaxed cloud screening for channels 6 - 8 and a relaxed orography screening for channels 5 - 6, excluding Antarctica, and this combination showed a small improvement in Northern Hemisphere forecast scores, and improved fits of short-range forecasts to ATMS channels 7 - 14. This combination of new observation errors and relaxed screening was introduced into the ECMWF model cycle 41R2.

1 Introduction

In Numerical Weather Prediction (NWP), data assimilation is the technique used to estimate the current state of the atmosphere, from which forecasts can be made. Observations and model background (prior estimates of the atmospheric state) are combined together in an optimal way to produce an estimation, known as the analysis. The weight given to observations is determined by the observation error covariance matrix, \mathbf{R} , and the weight of the background is determined by the background error covariance matrix, \mathbf{B} . An accurate representation of these two matrices is crucial for an accurate analysis of the atmospheric state.

The observation error covariance matrix for a given set of observations should include instrument noise, forward model errors, and representivity errors. The instrument noise may be a constant term for each instrument but forward model and representivity errors depend on the state of the atmosphere and the surface and so may vary for different measurements made under different atmospheric and surface conditions. Usually constant observation errors are assumed in assimilation systems. However, work is ongoing to more accurately represent the observation errors of different instruments. For example [Geer and Bauer \(2011\)](#) developed an observation error model for microwave imagers assimilated in all-sky conditions which varies with cloud amount, in order to account for increased representivity and model errors in cloudy situations. [Salonen et al. \(2015\)](#) also developed new observation errors based on background departures for the assimilation of Atmospheric Motion Vectors (AMVs), which included height-assignment error terms.

This report concerns the development of a more accurate observation error covariance matrix for the assimilation of the Advanced Microwave Sounding Unit -A (AMSU-A) instrument in the ECMWF Numerical Weather Prediction (NWP) system. AMSU-A is an important instrument for NWP because it provides very good global

coverage both due to the fact that the data can be used in a variety of atmospheric and surface conditions (cloud, sea-ice, etc.) and because there are currently 6 operational AMSU-A instruments onboard 6 different satellites, each of which has a different equatorial crossing time and samples a different period of the diurnal cycle. Currently, constant observation errors are used, values of which vary between channels but are the same for each instrument. Previously [Bormann and Bauer \(2010\)](#) estimated the observation errors for NOAA-18 AMSU-A using the Desroziers and Hollingsworth-Lonnberg methods and found values which were very close to instrument noise terms for most channels, indicating that the instrument noise dominates the observation error for most channels. The main sources of error in the forward model for AMSU-A are expected to be due to inaccuracies in cloud screening and emissivity estimation over land and sea-ice, which affect the lower peaking channels.

In this study we develop new observation errors for AMSU-A which include constant terms for all channels, and two situation-dependent terms for cloud- and surface-sensitive channels (channels 5 - 8). The situation-dependent terms are designed to include forward model errors due firstly to inaccurate cloud detection and secondly to uncertainties in the emissivity estimates, which together are thought to be dominant sources of forward model error for these channels. The constant terms can be considered to include all other sources of uncertainty, including in particular instrument noise. Different constant terms are calculated for different satellite and channel combinations, in order to reflect differences in instrument noise between channels and satellite instruments.

The observation errors are derived in all cases using background departure statistics. For the emissivity error term we employ a physically-based equation, derived from a simplified radiative transfer model following the method of [English \(2008\)](#), with emissivity errors estimated for different surface types from background departure statistics. The cloud liquid water term, applied over ocean only, is modelled as a function of the liquid water path calculated from AMSU-A window channel observations, and an empirical equation is used, which is derived from background departure statistics. The constant terms are derived by first calculating observation errors for each satellite and channel combination, following the method of [\(Desroziers et al., 2005\)](#), and then multiplying these values by inflation factors such that the average observation error for each channel is the same as values currently used in operations. After combining the three terms together the new observation errors have approximately the same global average values for each channel, but they vary for each satellite and for different atmospheric and surface conditions. Future work could investigate whether the observation errors should be reduced or increased, but as a first step we aim to keep the average observation error the same, but re-weight the observations depending on relative instrument noise and atmospheric and surface conditions.

The new observation errors were tested in assimilation trials. Trials were run firstly for the new observation errors, using the operational cloud, orography and sea-ice screening for AMSU-A tropospheric channels. To further test the new forward model observation errors, trials were then run relaxing the current tight screening over high orography, sea-ice and cloudy areas for the tropospheric channels.

This report is structured as follows. We present firstly a summary of the AMSU-A instrument and its assimilation at ECMWF, secondly the new observation errors are presented and thirdly results of assimilation trials testing these observation errors are presented. This report may be considered a follow-on to [Lawrence and Bormann \(2014\)](#), which was written before the study was fully completed. In this report we summarise the final results and conclusions, describing also the final configuration chosen as a contribution to the next ECMWF model cycle, 41R2.

2 AMSU-A

There are 10 different sounding channels on AMSU-A with frequencies around the 50 - 60 GHz oxygen absorption band and the radiances from these channels are sensitive to different parts of the troposphere and stratosphere. Channels 5 - 8 have weighting functions which peak in the troposphere, channel 9 in the tropopause and channels 10 - 14 in the stratosphere. The sensitivity of each sounding channel to different heights is illustrated by their clear-sky temperature Jacobians, shown in Fig. 1. Note that these Jacobians are normalised by the change in the natural logarithm of pressure for each model level ($\Delta \ln p$). As well as these sounding channels, AMSU-A has five channels with strong surface sensitivity which may be considered window channels: at 23.8 GHz, 31.4 GHz, 50.3 GHz, 52.8 GHz and 89 GHz. These channels are used for cloud-detection and emissivity estimation. Radiances are operationally assimilated from 6 different AMSU-A instruments flown on different platforms, including NOAA-15, NOAA-18, NOAA-19, MetOp-A, MetOp-B and Aqua. For some periods considered in this study a seventh instrument, NOAA-16, was also actively assimilated but this instrument failed in June 2014.

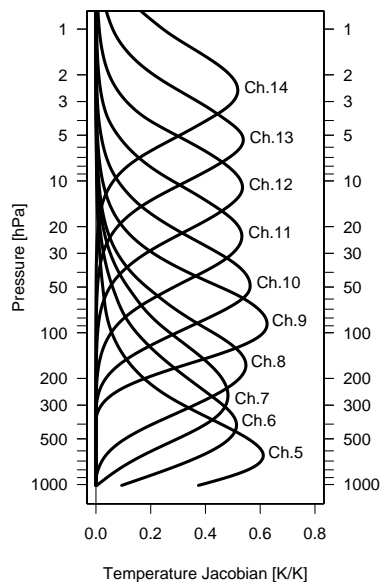


Figure 1: Clear-sky Temperature Jacobians for AMSU-A assimilated channels.

Channels 5 - 14 of AMSU-A are actively assimilated, after quality control. The different quality control checks applied are summarised in Table 1. Before assimilation, a cloud screening is applied to channels 5 - 8. Channels 5 - 7 are screened globally for cloud and channel 8 is screened for cloud in the Tropics only (at latitudes between 30°S and 30°N). This is because in the Tropics clouds are present at higher altitudes and so could affect channel 8 radiances. The cloud screening combines a background departure check of a window channel with a liquid water path check over ocean and scatter index check over snow-free land. The thresholds for these checks are given in Table 1. An orography screen is also applied over land for channels 5 and 6, as described in Table 1. This screen is applied since we have uncertainties in the skin temperature and emissivity estimates over land which we expect to dominate the atmospheric signal over high orography. Different thresholds are applied in the Tropics and the extra-Tropics to account for different surface-to-space transmittances. Additionally channel 5 is not used over land or sea-ice in the South Pole (at latitudes below 60°S), the 6 edge scan positions are not used. In practice this latter check rejects very little data. Additionally, variational quality control (Varqc) is applied to all channels, as is done for all instruments at ECMWF. This identifies data which may be considered outliers and downweights them by increasing observation error (Andersson and Jarvinen, 1998). Finally, as

with all satellite instruments, the data is thinned before being assimilated in order to avoid spatially correlated observation errors. AMSU-A is thinned to 125 km.

To illustrate the usage of AMSU-A after screening, Fig. 2 shows the used data for channels 5 - 8 for one NWP model cycle in the Northern Hemisphere winter (1 February 2014 21:00 - 03:00 UTC). Note that the lack of channel 5 - 7 data over Russia is due to the background departure check of the cloud screen flagging data over snow as cloudy. This is because the magnitude of channel 4 background departures increases when the land is covered by snow. In such situations the background departure check cannot distinguish between cloudy and snow-covered scenes and so rejects both.

Table 1: Screening applied operationally to AMSU-A channels 5 - 8 (ECMWF cycle 41R1)

	channels	surface type	latitude	Threshold for rejecting data
Cloud screening	5 - 8	Ocean	$ \text{lat} < 30$ (ch. 8)	$ o - b _{50.3\text{GHz}} > 3 \text{ K}$ or $lwp > 0.3 \text{ kg/m}^2$
		Land & Sea-ice	$ \text{lat} < 30$ (ch. 8)	$ o - b _{52.8\text{GHz}} > 0.7 \text{ K}$ or $SI > 3.0 \text{ K}$ over snow-free land
Orography screening	5	Land	$ \text{lat} \leq 30$ $ \text{lat} > 30$	orography > 1000 orography > 500
	6	Land	$ \text{lat} \leq 30$ $ \text{lat} > 30$	orography > 2000 orography > 1500
South Pole screening	5	Land & Sea-ice	$\text{lat} < -60$	reject all data
Scan Angle blacklisting	5 - 14	All	All	Reject data with scan positions of 1 - 3 or 28 - 30
Emissivity ‘realistic value check’	5 - 7	Land & Sea-ice	All	ϵ_{retr} and $\epsilon_{atlas} \leq 0.01$ or ϵ_{retr} and $\epsilon_{atlas} > 1.0$
Emissivity atlas check	5 - 7	Land	All	$ \epsilon_{retr} - \epsilon_{atlas} \geq 0.2$

For the lower peaking sounding channels (channels 5 - 8) which are sensitive to the surface we require estimates of surface emissivity and skin temperature for the radiative transfer forward model. Over ocean, the surface emissivity is calculated at each iteration from the analysed wind and surface temperature fields using the FASTEM v6 model (English and Hewison, 1998, Liu et al., 2011, Kazumori and English, 2014). Over land and sea-ice, however, the surface emissivity is calculated from the observed brightness temperatures of channel 3 (50.3 GHz), using the radiative transfer equations of RTTOV with atmospheric and skin temperature terms fixed by background values (Karbou et al., 2006). A dynamic emissivity atlas is also maintained over land, which is used to check the validity of the calculated value. This atlas is updated from previous retrievals using a Kalman filter and if the retrieved value differs by 0.2 from the atlas value then the atlas is used. In practice the atlas emissivity is used very rarely - for less than 1% of data. An additional emissivity check that the value is realistic is applied, as described in Table 1. A sink variable is used for the skin temperature: during assimilation a value is retrieved for each observation point, with an applied observation error of 5 K over land, 7.5 K over

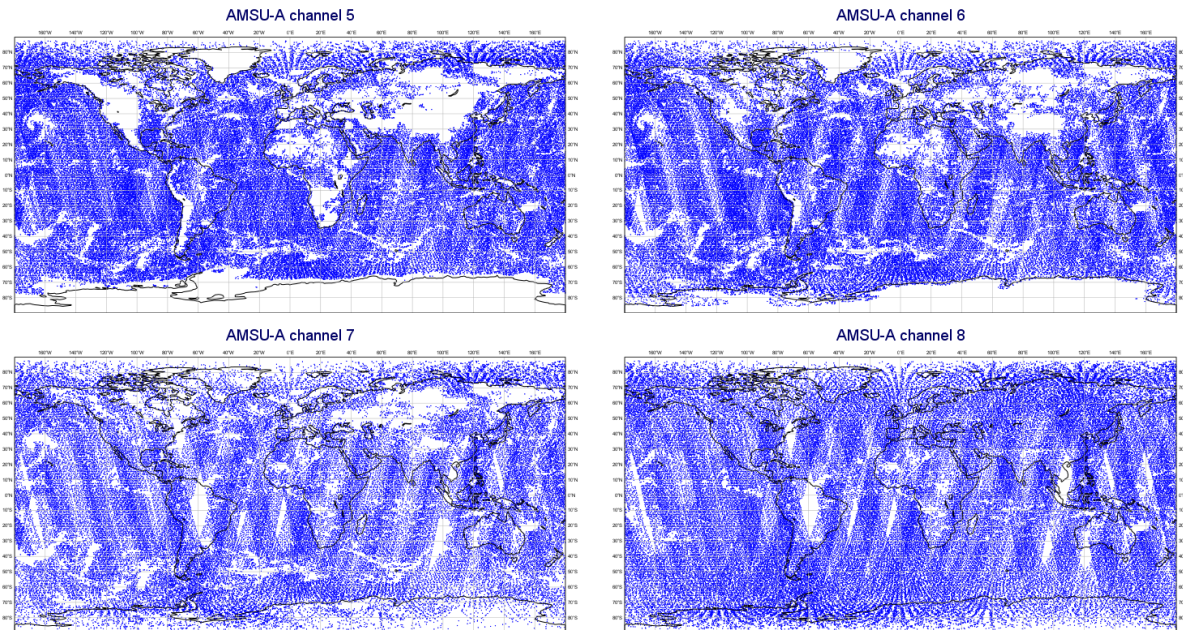


Figure 2: Geographic coverage of AMSU-A data assimilated for one cycle of the ECMWF NWP model on 1 February 2014, channels 5 - 8.

sea-ice, and 3 K over sea. The background value is taken from the model.

In order to assimilate the data, a Variational Bias Correction scheme (VarBC) is applied to channels 5 - 13 (Dee (2004), Auligné et al. (2007)). Channel 14 is used without a bias correction so that it can anchor the stratospheric temperature analysis: using channel 14 with a variational bias correction leads to an undesired drift in bias correction due to interactions between model bias and VarBC.

When AMSU-A data passes cloud-screening and additional quality control checks it is assimilated with observation errors given in Table 2.

Table 2: Observation Errors used operationally for AMSU-A = σ_{op}

Channel number	σ_{op}
5	0.28
6	0.20
7	0.20
8	0.20
9	0.20
10	0.24
11	0.35
12	0.50
13	0.85
14	1.40

Note that not all channels of all satellites are used. Some channels have been blacklisted due to steadily increasing noise, spikes in the standard deviation of background departures, channel failure, etc. Blacklisted channels, as of December 2014, are given in Table 3.

Table 3: AMSU-A channels blacklisted operationally (as of December 2014). Channels are blacklisted globally, unless stated otherwise.

Satellite	Channels
NOAA-15	6, 11, 14
NOAA-16	5 - 7 over land & sea-ice, 8, 9
NOAA-18	none
NOAA-19	7, 8
MetOp-A	7, 8
MetOp-B	none
Aqua	5, 6 over land & sea-ice, 7 globally, 8 over land in the Tropics

3 New Observation Errors

The new observation errors have three components: a constant term, $\sigma_{constant}$, an emissivity error term, σ_{emis} , and a cloud liquid water term which is calculated as a function of the liquid water path (lwp), σ_{lwp} . They are combined as follows:

$$\sigma_o^2 = \sigma_{constant}^2 + \sigma_{emis}^2 + \sigma_{lwp}^2. \quad (1)$$

Note that for channels with no surface or cloud sensitivity, σ_{emis} and σ_{lwp} are zero, and over land σ_{lwp} is zero since the liquid water path cannot be derived from AMSU-A observations over land. Instead we will rely on the tight cloud-screening over land (see Table 1) to remove all cloud-affected data. The constant term in this equation may be considered to include all other sources of observation error including instrument noise, representivity, and spectroscopy errors. The derivation of each term is described in the following.

3.1 Estimates of the constant term from Desroziers-derived observation errors

Desroziers et al. (2005) showed that observation-error covariance matrices can be diagnosed from the following relationship, assuming data-assimilation schemes follow linear estimation theory, and the (operationally) assigned weights are consistent with the true weights:

$$\tilde{\mathbf{R}} = E [\mathbf{d}_a, \mathbf{d}_b^T], \quad (2)$$

where \mathbf{d}_b are the background departures of the observations, \mathbf{d}_a are the analysis departures of the observations and $E[\cdot]$ is the expectation operator. Assuming no error correlation, the R matrix is diagonal and the observation error for a given channel, $\sigma_{Desroziers}$, can therefore be calculated as:

$$\sigma_{Desroziers}^2 = \overline{(o-a)(o-b)} - \overline{(o-a)}\overline{(o-b)} \quad (3)$$

Current observation errors for the different AMSU-A channels are slightly larger than the Desroziers-derived values. Table 4 shows the Desroziers-derived values, together with inflation factors for the currently assumed observation errors.

We calculated new Desroziers-derived observation errors from (3) for each satellite-channel combination and then multiplied these terms by the inflation factors given in Table 4 in order to obtain values for the constant

Table 4: Desroziers-derived observation errors for each channel, $= \sigma_{desroziers}$, and the Inflation factors $= \sigma_{op}/\sigma_{desroziers}$ for each channel

Channel number	$\sigma_{desroziers}$	Inflation Factor $= \sigma_{op}/\sigma_{desroziers}$
5	0.18	1.60
6	0.15	1.32
7	0.15	1.37
8	0.17	1.20
9	0.16	1.26
10	0.20	1.23
11	0.23	1.54
12	0.33	1.51
13	0.48	1.79
14	0.85	1.66

observation error terms. Mathematically, this can be expressed as follows:

$$\sigma_{constant}(i, j) = \sigma_{Desroziers}(i, j) * \frac{\sigma_{op}(j)}{\sigma_{Desroziers}(j)}, \quad (4)$$

where $\sigma_{constant}(i, j)$ is the new constant term for a given satellite i and channel j , $\sigma_{Desroziers}(i, j)$ is the Desroziers-derived observation error for that satellite and channel, calculated from (3), $\sigma_{op}(j)$ is the current observation error used for channel j and $\sigma_{Desroziers}(j)$ is the Desroziers-derived observation error for channel j , calculated from (3) using data from all instruments. Multiplying the Desroziers-derived observation errors by the inflation factors allows us to keep the same average observation error for each channel, and the only effect is to change the relative weighting of each satellite-channel combination.

New constant observation error terms were calculated for channels 5 - 13 for the different AMSU-A instruments used at ECMWF, which include instruments onboard MetOp-A, MetOp-B, NOAA-15, NOAA-16 (used up to June 2014), NOAA-18, NOAA-19 and Aqua. Values were calculated for used data (data passing screening and actively assimilated) in a sample data-set for a 3 month period, combining January, April and May 2014. This sample dataset included only used data (data actively assimilated) for all channels and additionally only data over ocean, with liquid water path values $\leq 0.05 \text{ kg/m}^3$, for channels 5 - 8. This latter condition was applied so that emissivity and cloud liquid water observation error terms could be considered negligible ($<0.01 \text{ K}$). Note that new observation errors were not calculated for satellite-channel combinations which are currently black-listed. Additionally, new observation errors were not calculated for channel 14. This is because this channel has a non-zero mean background departure due to the fact that bias correction is not applied. Calculating new observation errors using the method outlined above led to a significant reduction in the average observation error because of the non-zero mean.

The new observation error constant terms are given in Table 5 and the spread of new values is shown graphically in Fig. 3a) along with the current operational observation errors and post-launch estimated noise (NEAT). These latter values are provided courtesy of Nigel Atkinson (UK Met Office) and are from July 2011 for NOAA-16 and February 2015 for all other instruments. Qualitatively the new observation error terms follow NEAT statistics for these instruments. For example MetOp-A has the highest NEAT for channels 11 - 13 and also the highest observation errors. The new observation errors also follow more accurately the channel variation of the NEAT values as illustrated for NOAA-18 in Fig. 3b). Furthermore, the (old) operational observation errors are lower than the estimated instrument noise in some cases and the new observation errors correct this. The biggest individual change in observation errors is the increase for Aqua AMSU-A channel 6 from 0.20 K to 0.31 K.

This satellite instrument has the highest noise for this channel.

Table 5: New Observation Errors for AMSU-A instruments, and the range of values for each channel

Channel	MetOp-A	MetOp-B	NOAA-15	NOAA-16	NOAA-18	NOAA-19	Aqua	Range
5	0.30	0.27	0.25	0.24	0.33	0.27	-	0.09
6	0.18	0.18	-	0.17	0.19	0.18	0.31	0.14
7	-	0.19	0.18	0.18	0.23	-	-	0.05
8	-	0.20	0.15	-	0.25	-	0.18	0.10
9	0.21	0.19	0.21	-	0.20	0.20	0.19	0.02
10	0.26	0.24	0.22	0.23	0.24	0.25	0.23	0.04
11	0.39	0.34	-	0.33	0.35	0.34	0.33	0.06
12	0.54	0.50	0.47	0.49	0.49	0.50	0.48	0.07
13	0.93	0.84	0.81	0.83	0.84	0.86	0.82	0.12

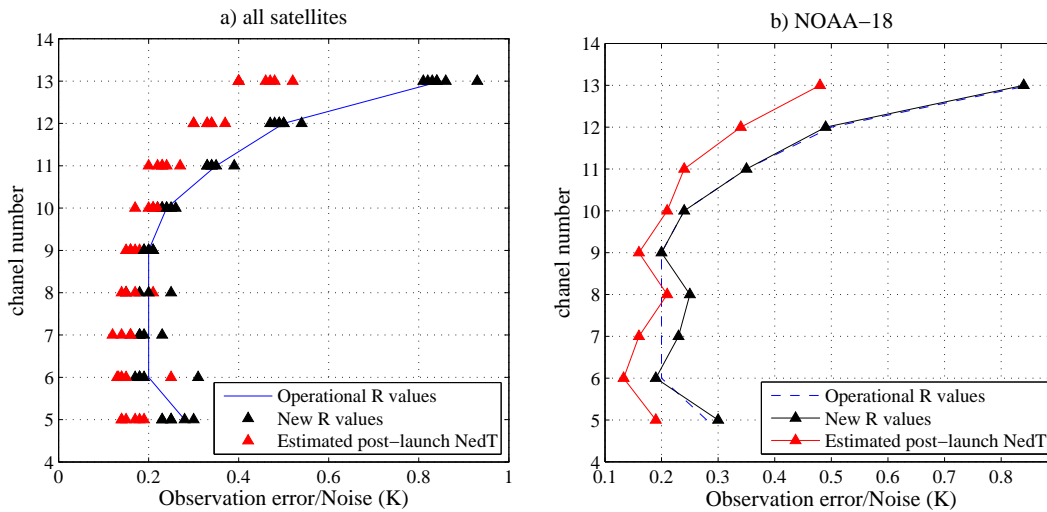


Figure 3: Operational observation errors, new observation errors and estimated post-launch instrument noise for a) all AMSU-A instruments onboard different satellites, and b) NOAA-18 AMSU-A, as a function of channel number.

3.2 Emissivity forward model errors for surface-sensitive channels

The derivation of emissivity forward model errors has been previously presented by Lawrence and Bormann (2014). Here we summarise the derivation of the emissivity observation error term and explain in more detail the estimation of the emissivity error itself.

The emissivity observation error term, σ_{emis} , derived from simplified radiative transfer equations, can be expressed as (Lawrence and Bormann, 2014, English, 2008):

$$\sigma_{emis}^2 \approx T_s^2 \Gamma^4 \overline{(\delta \epsilon)^2}, \tag{5}$$

where T_s is the skin temperature, Γ is the surface-to-space transmittance, ϵ is the surface emissivity, and $\overline{(\delta \epsilon)^2}$ the mean square emissivity error. In deriving this equation, we have assumed an isothermal atmosphere whose temperature is approximately equal to the skin temperature. (5) is a physically-based equation for the observation errors which increases with surface-to-space transmittance, skin temperature and emissivity error, i.e.

observation errors are higher where the sensitivity to the surface is higher and for higher surface temperatures. $\overline{(\delta\epsilon)^2}$ may vary with surface type which means that the observation errors will be different for different surface types.

In order to estimate $\overline{(\delta\epsilon)^2}$ we calculated a best fit of (5) combined with (1) and a liquid cloud term of zero, i.e. a best fit of the following:

$$\sigma_o^2 = T_s^2 \Gamma^4 \overline{(\delta\epsilon)^2} + \sigma_{constant}^2, \quad (6)$$

where the mean square of background departures of channel 5 were used as a proxy for σ_o^2 , model background values were used for T_s and Γ and the fit was weighted by the number of data. Note that the constant term was included here in order to estimate the emissivity errors but was not used as the constant term of the final observation errors. A best fit of (6) was calculated for each satellite instrument and 4 different surface types: snow-free land, snow-covered land, sea-ice and ocean. Over ocean, only data with a liquid water path ≤ 0.05 kg/m³ were included, to keep cloud liquid water errors negligible, and justify setting $\sigma_{lwp} = 0$. Previously [Di Tomaso and Bormann \(2013\)](#) calculated emissivity error values in a similar way for different land surfaces, including forest, desert, etc., but all snow-free surfaces were found to have similar values and so it was decided to combine these into one surface type. Note that using the background departures as a proxy for observation errors in (6) is an approximation since the background departures also include skin temperature errors and background errors of atmospheric terms as well as other observation error terms, including representivity and errors due to undetected cloud. Additionally background departures over ocean include background errors for the surface wind speed.

Different estimated emissivity error values were calculated for different satellites, and the variation in values is given in Table 6. Fig. 4 also shows the root mean square background departures for each satellite instrument as a function of $T_s \Gamma^2$, the slopes of which indicate the emissivity errors. For land and sea-ice we might expect different emissivity errors for different satellites given that the emissivities are calculated from channel 3 observations, which will have different noise values for different satellites, and also the skin temperature error may vary depending on the diurnal cycle. Over ocean we would not expect to have a variation in emissivity error, since it is calculated from the FASTEM model rather than being retrieved from observations. Any variations found, therefore, are more likely to be due to different background errors for different times of the diurnal cycle, which we would not want to include in the observation errors.

Table 6: Emissivity errors for different surface types

Surface Type	Range of $(\delta\epsilon)^2$ for different satellites	final $\overline{(\delta\epsilon)^2}$
Ocean	0.01 - 0.02	0.015 ²
Sea-ice	0.04 - 0.05	0.050 ²
Snow-covered land	0.025 - 0.056	0.050 ²
Snow-free land	0.018 - 0.022	0.022 ²

In general, the range of different estimated emissivity errors for the different satellites is quite small, with the exception of snow-covered land. Over snow there is a clear difference between NOAA-15 and NOAA-18 AMSU-A, which have similar slopes and the other satellite instruments which have lower slopes. This difference was diagnosed to be due to the scaling of the surface-to-space transmittance which is applied in the ECMWF assimilation system for NOAA-15 and NOAA-18 AMSU-A. Scaling factors, known as γ factors, were previously developed for AMSU-A in order to correct forward-model biases, due to spectroscopy or pass-band shift errors ([Watts and McNally, 2004](#), [Di Tomaso and Bormann, 2011](#)). While this factor reduces the standard deviation of background departures globally, it does not affect background departures in high latitudes.

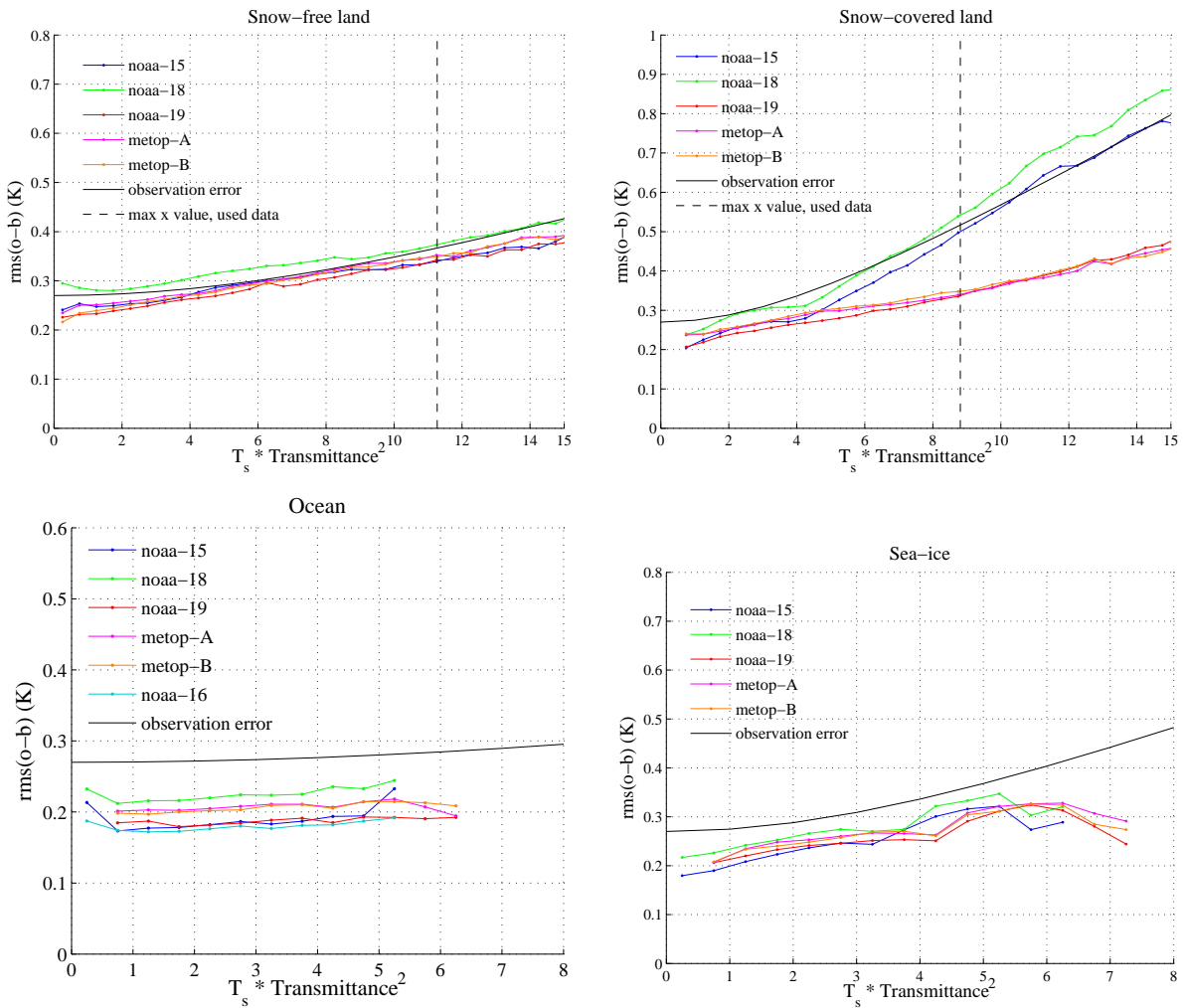


Figure 4: root mean square background departures averaged over 2 months and plotted as a function of $x = T_s \Gamma^2$ for binned x values where the size of the bin is 0.5 plotted for snow-free land, snow-covered land, ocean and sea-ice. The new observation errors are also shown as a dashed line, with a noise term of 0.27 K.

Consequently, for the satellites with a γ correction the surface-to-space transmittance is reduced by the γ factor over snow-covered land, while standard deviation of background departures remains unchanged and hence we have higher gradients for these satellites.

For the new emissivity observation error term, we chose to use the same emissivity errors for all satellites, for simplicity, and the values chosen are given in Table 6 (column 3). For land and sea-ice we chose values at the top of the estimated range given in Table 6. This was done partly to be cautious and partly because we expect to have error correlations between the background skin temperature and the emissivity error, which are not accounted for, and so using higher observation errors could compensate for this effect. For the ocean emissivity error we chose to take the average value, rather than the highest. This is because, unlike over land and sea-ice, we do not expect to have correlations with the skin temperature errors and, furthermore, the values of Table 6 (column 2) indicate that the emissivity errors are generally lower over ocean than over snow-free land.

The new emissivity observation error term is very small for channels 6 and above of AMSU-A, due to their low surface-to-space transmittance. For channel 6 the emissivity error term is less than 0.01 K for 95% of all data (before screening) and less than 0.01 K for almost 100% of channel 7 data. The emissivity error term therefore mainly affects channel 5. The emissivity error term affects the global mean observation error of channel 5 by very little (~ 0.01 K) but it does introduce a variation depending on surface type and atmospheric conditions. This is illustrated in Fig. 5 which shows histograms of channel 5 observation errors calculated from (6) with $\sigma_{constant} = 0.27$ K for different surface types, and by Fig. 6 which shows the geographic pattern of the same observation errors. As Fig. 6 shows, observation errors are higher over land and sea-ice than over ocean, and are higher at the centre of the swath, where the surface-to-space transmittance is higher. In some areas, the observation errors are significant in comparison to the instrument noise. These figures also show that the current orography and sea-ice screening removes data with the highest observation errors.

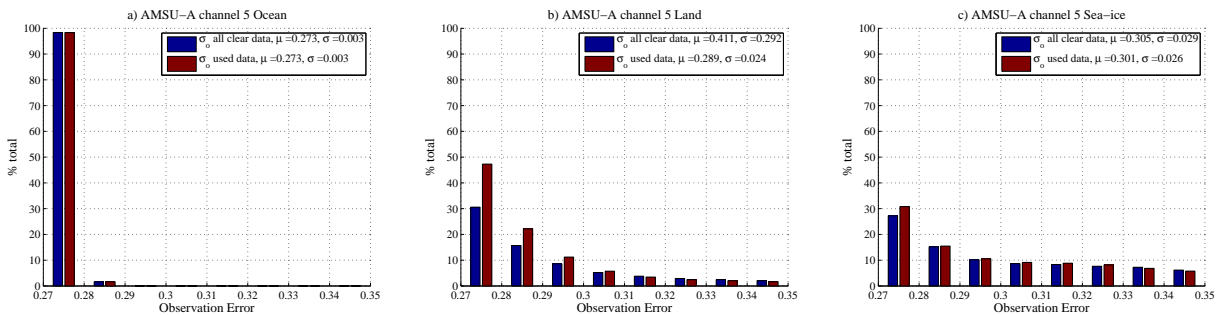


Figure 5: Histograms of the new emissivity observation error terms combined with a constant observation error term of 0.27 K for channel 5 over a) Ocean, b) Land and c) sea-ice. Values are shown for all data after cloud screening and thinning and for used data (the data assimilated). The mean (μ) and standard deviations (σ) of observation errors are indicated in the legend.

3.3 Cloud liquid water observation error terms

Cloud can affect AMSU-A radiances due to absorption/emission of liquid water and scattering of ice particles. AMSU-A is currently assimilated in clear-sky conditions only and the forward model used in this assimilation is RTTOV which does not account for cloud effects. At ECMWF, some satellites are assimilated in all-sky conditions and in this case the effects of clouds are accounted for in the forward model used for all-sky instruments: RTTOV-SCATT. The aim of developing a cloud liquid water path observation error term for AMSU-A is to continue using AMSU-A in the clear-sky stream but account for forward model errors in the presence of cloud by including an additional term in the observation errors. Previously all-sky assimilation of AMSU-A

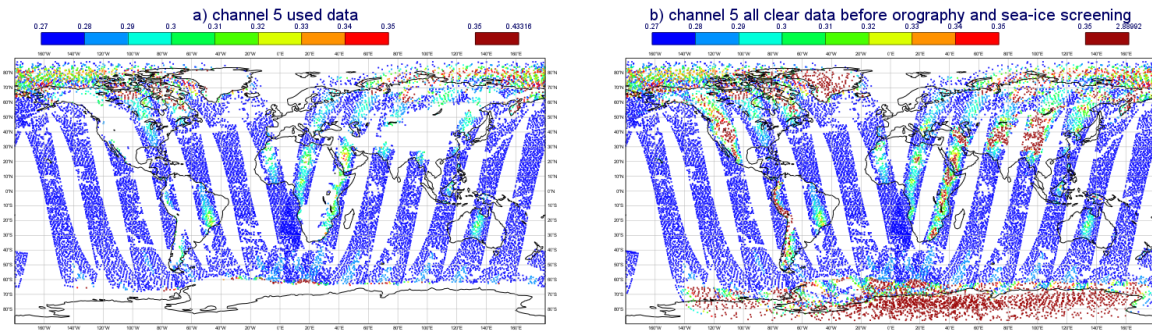


Figure 6: New observation errors for MetOp-B AMSU-A channel 5 for one cycle of the assimilation in the Northern Hemisphere summer (1 June 2014, 0z cycle) for a) used data and b) all clear data before orography and sea-ice screening

channel 4 was tested but it was found that cloud effects were aliased into temperature increments, degrading the temperature analysis (Geer et al., 2012).

In applying this approach we represent the variability of AMSU-A observations in the presence of clouds as a random error. However, in the presence of cloud non-zero mean background departures, or biases, can also be observed. In areas of strong scattering in the Tropics a strong negative bias is observed (up to -1.0 K) and in areas of high liquid water path in the extra-Tropics a positive bias is observed (up to 0.5 K). When these biases are too large they may introduce local temperature biases, even if the data is assigned a larger observation error. We will therefore keep a cloud screen to remove the worst-affected data, and rely on increased observation errors to downweight the remaining biased data.

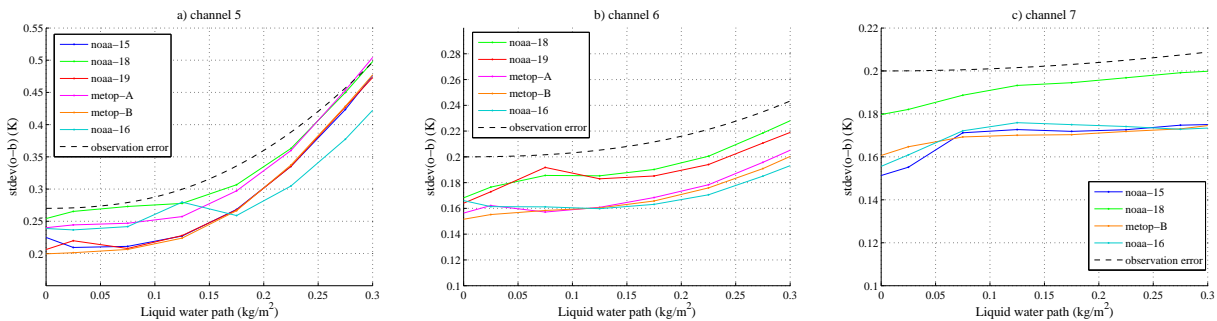


Figure 7: Standard deviation of clear-sky background departures as a function of liquid water path (blue triangles) for channels 5 - 7 of AMSU-A. Also shown are the best fits (black dashed line), combined with noise terms of 0.27 K for channel 5 and 0.20 K for channels 6 and 7.

A cloud observation error term was derived for AMSU-A channels 5 - 7 from empirical best fits of the standard deviation of background departures to the cloud liquid water path, which is calculated from AMSU-A window channel observations (Lawrence and Bormann, 2014). Background departure statistics appeared to follow a quadratic-type relationship with liquid water path (lwp) for channels 5 - 6. This can be seen in Fig. 7, which shows the standard deviation of background departures as a function of binned AMSU-A liquid water path for channels 5 - 7, averaged over 1 month of data. The different solid lines in these figures indicate values for different satellites and the standard deviation of background departures is calculated for liquid water paths binned in intervals of 0.05 kg/m². A weak relationship between the standard deviation of background departures and cloud liquid water path can also be observed for channel 7 (Fig. 7c). This relationship appears to have two regimes with different slopes, which is interesting. As channel 7 peaks at a higher altitude (~400hPa) the relationship to liquid water path shown in Fig. 7 may be due to a correlation between liquid water path and

scattering from ice cloud. There could also be competing effects of absorption/emission from super-cooled liquid water and scattering from ice cloud, which might lead to the two regimes observed in Fig. 7.

Given the observed relationships between background departures and liquid water path, quadratic equations were chosen for the cloud liquid water observation error terms of channels 5 - 6. For channel 7 we chose to use a simple observation error model of a linear equation. This is an approximation since the relationship does not appear to be linear.

Replacing σ_{lwp} in (1) by a quadratic or linear equation, and assuming $\sigma_{emis} \approx 0$ over ocean, (1) can therefore be rewritten as follows, for channels 5 - 7 over ocean:

channel 5 - 6:

$$\sigma_o^2 = \sigma_{constant}^2 + (Alwp^2 + Blwp)^2, \quad (7)$$

channel 7:

$$\sigma_o^2 = \sigma_{constant}^2 + (Blwp)^2, \quad (8)$$

for constants A and B , and a constant observation error term $\sigma_{constant}$. Best fits of (7) and (8) were calculated using the standard deviation of background departures over ocean as a proxy for σ_o . As for the emissivity observation error term, the constant term was included in order to accurately derive a relationship for the liquid water path observation error term, but was not included in the final observation errors. Best fits were calculated for different satellites and then the one with the highest slope was chosen.

The final derived best fits are:

channel 5:

$$\sigma_{lwp} = 2.0lwp^2 + 0.79lwp, \quad (9)$$

channel 6:

$$\sigma_{lwp} = 0.54lwp^2 + 0.30lwp, \quad (10)$$

channel 7:

$$\sigma_{lwp} = 0.20lwp. \quad (11)$$

The best fits of (9) - (11) are also plotted in figure 7 as the dashed black line, combined with a constant observation error term of $\sigma_{constant} = 0.27$ K for channel 5 and $\sigma_{constant} = 0.20$ K for channels 6 and 7. Best fits were calculated for all data, before cloud-screening. If calculated for used data after cloud screening the standard deviation of background departures still increased with liquid water path but with a lower slope (results not shown). We decided to use observation error terms based on statistics for all data, to allow us to later change the cloud screening and introduce more data.

Fig. 8 shows the spread of the new cloud observation error terms, combined with constant terms of $\sigma_{constant} = 0.27$ K for channel 5 and $\sigma_{constant} = 0.20$ K for channels 6 and 7, both before and after the current operational cloud screening, and a new cloud screening proposed in section 5. Fig. 9 shows maps of the same observation errors. As with the emissivity observation error terms, the cloud liquid water terms do not greatly increase the global average of the observation error (by 0.01 K for channel 5, and less for channels 6 and 7) however there is now a situation-dependent variation in observation errors.

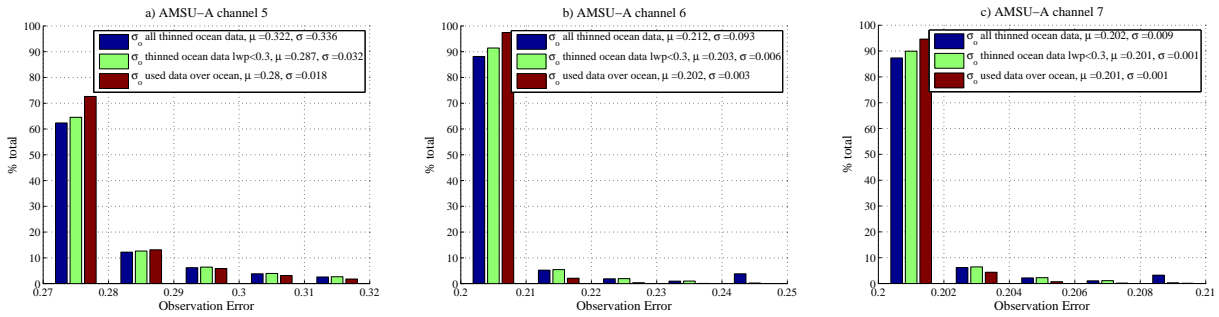


Figure 8: Histograms of the new lwp observation error terms combined for data over ocean, with constant noise terms for a) channel 5, combined with a noise of 0.27 K, b) channel 6 and c) channel 7 combined with noise terms of 0.20 K. Values are shown both for all ocean data after thinning and for used data over ocean (the data assimilated). The mean (μ) and standard deviations (σ) of observation errors are indicated in the legend.

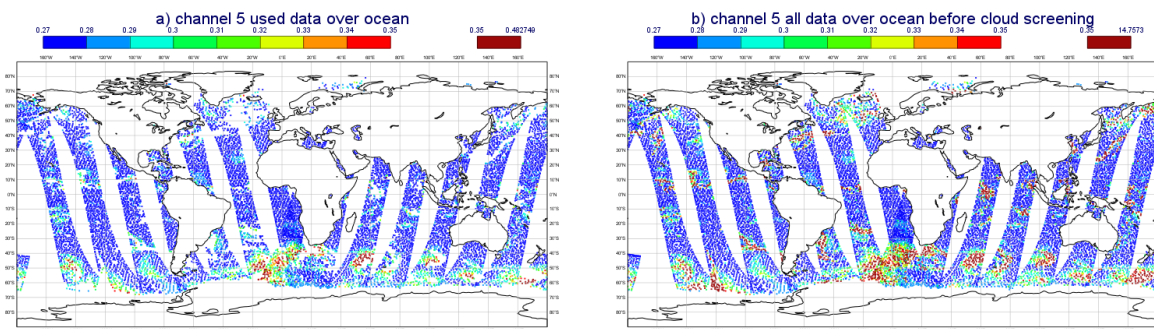


Figure 9: New lwp observation errors for MetOp-B AMSU-A for one cycle of the assimilation in the Northern Hemisphere summer (1 June 2014, 0z cycle) for a) channel 5 used data, b) channel 5 all data after thinning.

4 New AMSU-A Observation Errors

Combining all terms derived in sections 3.1, 3.2 and 3.3, the new observation errors for AMSU-A channels 5 - 13 can be written as:

$$\sigma_o^2 = \sigma_{constant}^2 + T_s^2 \Gamma^4 \overline{(\delta\varepsilon)^2} + \sigma_{lwp}^2, \quad (12)$$

where $\sigma_{constant}$ depends on the satellite and channel, and values are given in Table 5, and where σ_{lwp} is calculated as follows:

$$\sigma_{lwp} = \begin{cases} 2.0lwp^2 + 0.79lwp, & \text{for channel = 5 over ocean,} \\ 0.54lwp^2 + 0.30lwp, & \text{for channel = 6 over ocean.} \\ 0.20lwp, & \text{for channel = 7 over ocean,} \\ 0 & \text{else.} \end{cases} \quad (13)$$

Note that the emissivity error term of (12) is zero for channels 9 and above (since $\Gamma=0$), so for these channels the observation error reduces to $\sigma_o = \sigma_{constant}$. The global averages of the new observation errors remains the same as the operational values given in Table 2 except for channel 5 which is increased slightly from 0.28 K to 0.30 K. However, given this is a small increase the main effect is to introduce a variation depending on satellite and atmospheric and surface conditions, i.e. the observation errors are now both situation- and satellite-dependent. Fig. 10 illustrates the variation in the new observation errors for channels 5 - 7, showing values for MetOp-B AMSU-A before and after quality control.

5 Adding more data by relaxing the orography, sea-ice and cloud screening

Currently, AMSU-A channels 5 and 6 are blacklisted over high orography and channel 5 is blacklisted over the Southern Hemisphere sea-ice, due to the expected inaccuracy of the surface contribution in these areas. Given that we now have a surface term in the new observation errors it may be possible to re-introduce some of these data. This will also allow us to test the new observation errors more fully, since there will be more of a variation than for the operational screening. In adding more data over orography, we decided to replace the current orography screen with an observation error screen, in order to continue to filter out data with the highest observation errors, and to exclude data where the surface signal dominates the atmospheric signal. We chose to screen data where the emissivity error term (over land) was higher than 0.25 K for channel 5, or higher than 0.20 K for channel 6, which excludes data with surface-to-space transmittances higher than approximately 0.20 (depending on surface type, skin temperature...) and is also where the emissivity observation error term is approximately equal to the constant term of the observation error for these channels. This latter condition ensures that we do not introduce data where correlations between background and observation errors are high (which would be detrimental to the assimilation system). Since the emissivity observation error term relies on background values of surface-to-space transmittance and skin temperature it could introduce this correlation.

With the use of cloud observation errors, the cloud quality control for channels 5 - 8 could also be relaxed, allowing in more data which were previously screened. The current quality control for cloud includes a window channel background departure check which may be removing cloud-free data along with the cloudy data. With the new cloud observation errors we are attempting to represent liquid cloud effects as a random Gaussian distribution. Therefore with the new observation errors it is better to try and keep the whole distribution and

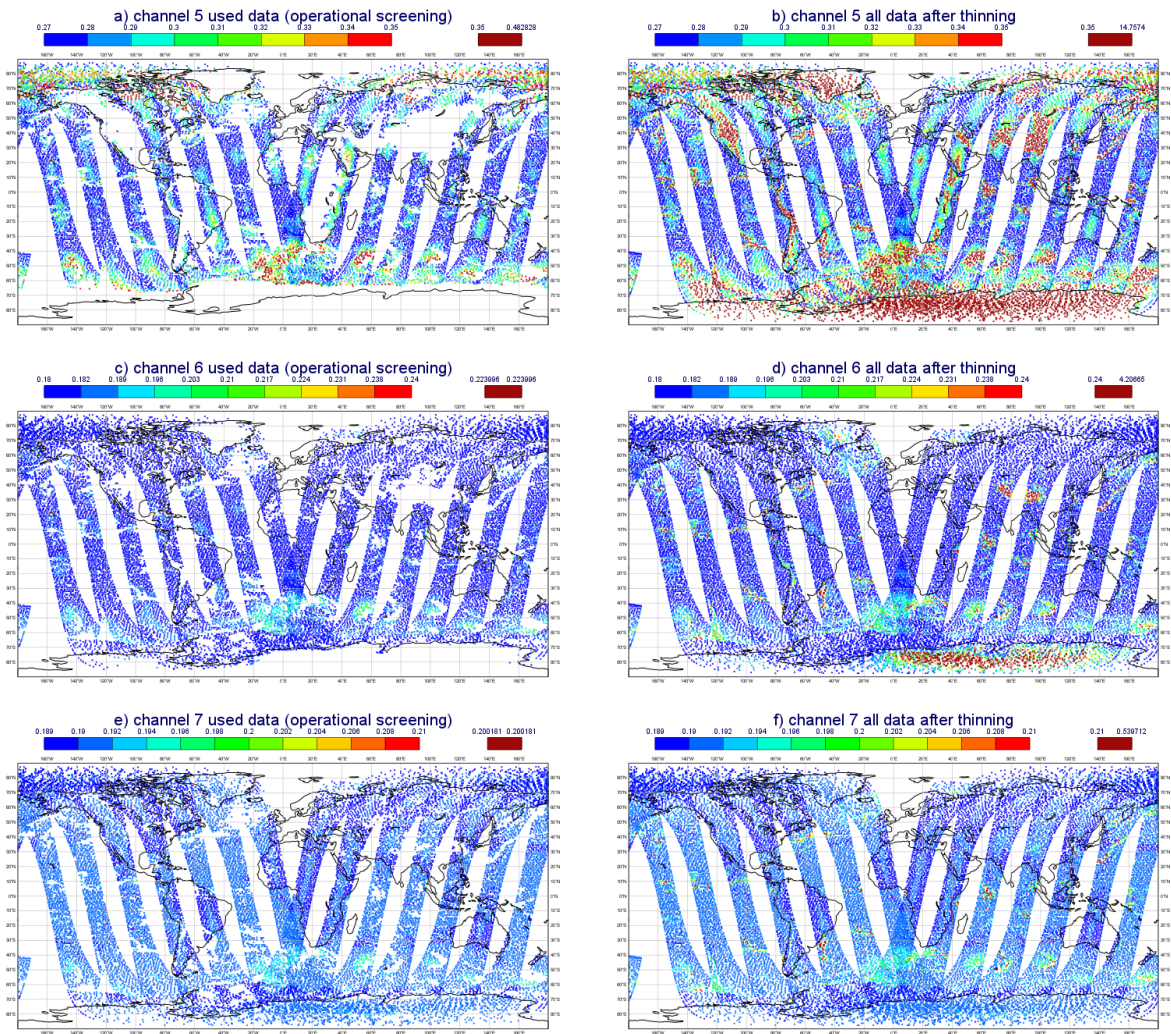


Figure 10: New observation errors for MetOp-B AMSU-A for one cycle of the assimilation in the Northern Hemisphere summer (1 June 2014, 0z cycle) for a) channel 5 used data, b) channel 5 all data after thinning, c) channel 6 used data, d) channel 6 data after thinning, e) channel 7 used data, and f) channel 7 data after thinning. Note the different scales for different channels.

rely on observation errors to downweight the data with higher background departures that are now allowed to pass screening. However we still wish to exclude data which are affected by strong scattering from ice clouds, since we have not included scattering effects in our observation error model, these data tend to have significant negative biases, and in any case there is not likely to be useful temperature information due to the strong scattering. We wish to therefore develop a new cloud screen based on a scattering index, which could replace the background departure check to allow in more data whilst screening data affected strongly by scattering from ice cloud.

A scattering index (SI) can be calculated over ocean from channel 1 (23 GHz) and channel 15 (89 Gz) observations, with an additional correction for water vapour, as:

$$SI = TB_{ch1} - TB_{ch15} - (TB_{ch1}^{clr} - TB_{ch15}^{clr}), \tag{14}$$

where TB_{ch1} and TB_{ch15} are the measured radiances of channels 1 and 15 respectively, both of which are not bias-corrected, and TB_{ch1}^{clr} and TB_{ch15}^{clr} are the clear-sky background radiances for channels 1 and 15 respectively. This scattering index relies on the fact that channel 15 is more strongly affected by scattering than channel 1 in order to identify scattering features. However, channels 1 and 15 are also affected differently by water vapour, due to the water vapour continuum, and so the $(TB_{ch1}^{clr} - TB_{ch15}^{clr})$ is included in order to correct for this.

In order to use the scattering index to remove cloud-scattering effects we need to define a threshold. A threshold of 5 K was chosen as it removes most of the negative departures of channel 5, removing all values less than approximately -1.7 K, while keeping the majority (98 - 99 %) of the data. This is shown in Fig. 11a). Channels 6 - 8 are less affected by cloud than channel 5, as can be seen by the scatter plot shown in Fig.11b) for channel 6, and so we could have a more relaxed screen for these channels. However this is left for future work.

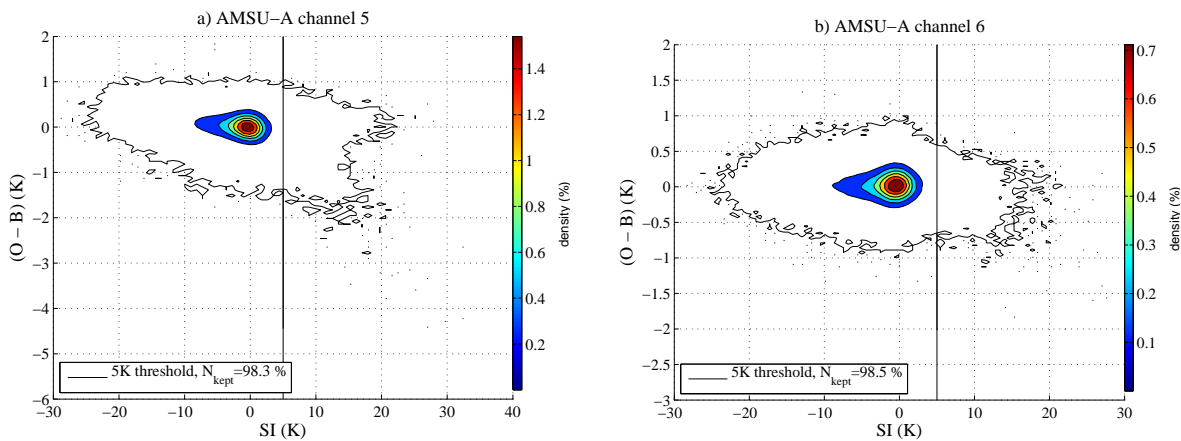


Figure 11: Scatter plots of background departures for 24-hours of AMSU-A data as a function of SI for channels a) 5 and b) 6.

The effect of the new cloud screening on the background departures is shown in Fig. 12a), which shows the distribution of background departures for channel 5 before and after screening and Fig. 12b) which shows the same plot normalised by observation errors. Note that the liquid water path check is kept with the new scattering index screen. The operational cloud screening reduces the standard deviation of background departures whereas the new cloud screening does not significantly reduce them, as shown in Fig. 12a). However when we normalise by the new observation errors the new cloud screen does reduce the spread of the histogram, as shown in Fig. 12b). Thus combining the new observation errors with the new cloud screening we are able to introduce more data, but weight it so that cloud effects are reduced.

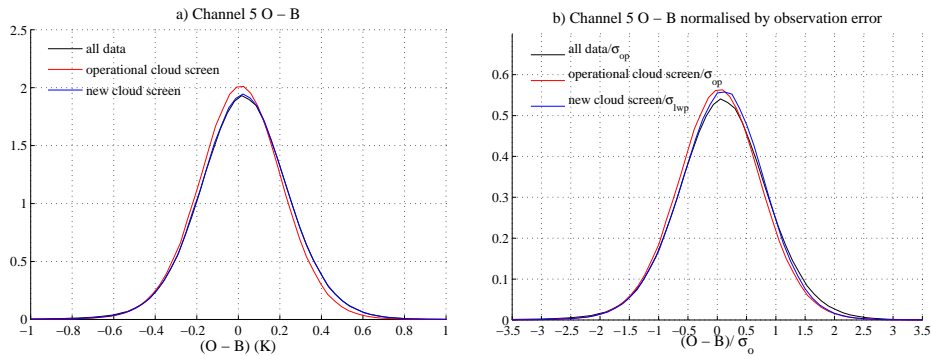


Figure 12: a) The distribution of background departures for channel 5 for all data, all data after operational cloud screening and all data after the new scattering index screen. b) The same as a) but values are normalised by observation errors. For all data and the operational cloud screen they are normalised by the operational observation errors and for the new cloud screen they are normalised by the new observation errors. This latter includes the cloud observation error term and a noise term of 0.27 K, and the average value is 0.28 K (the same as operations).

6 Assimilation Trials

Assimilation trials were run to test the new observation errors over summer and winter periods. Firstly the new observation errors were tested with no change in the operational screening. Secondly trials were run to further test the observation errors by relaxing the orography and sea-ice screening and to change the cloud screening. As a result of these tests, the new observation errors were combined with some screening changes, as a contribution to the new ECMWF model cycle, cycle 41R2, and this contribution was also tested. All results were compared to control experiments.

All assimilation trials were run using a recent version of the ECMWF model and at a lower horizontal resolution than the operational set-up. In order to assess the impact of the new observation errors on the accuracy of the forecasts, the change in fits of other observations to the background (short-range forecasts) as well as the change in forecast minus own analysis were assessed.

7 Results of assimilation trials

7.1 Testing new observation errors with operational screening

Firstly we tested the new observation errors without changing the screening. Trials were run over two 3 month periods for 1 February 2014 - 30 April 2014 and 1 June 2014 - 31 August 2014, with cycle 41R1 of the ECMWF model at a horizontal resolution of T639 and 137 levels in the vertical. In these trials the new AMSU-A observation errors defined by (12) - (13) and Table 5 were used. For comparison, control experiments were also run, which used the operational observation errors for AMSU-A, given in Table 2.

Results showed a mainly neutral impact on forecast scores, as shown in Fig. 13. A positive impact on background departures of ATMS channels 7 - 14 (equivalent to AMSU-A channels 6 - 14) was observed, however, as shown in Fig. 14 (black line). This is encouraging since it indicates an improved short-range forecast accuracy. This improvement was found to be due to the new satellite-dependent constant terms, since it was also observed in trials using only these terms (with $\sigma_{iwp} = 0$ and $\sigma_{emis} = 0$). This result is also shown in Fig. 14.

The effect of the new observation errors on the variational bias correction for AMSU-A was also checked and

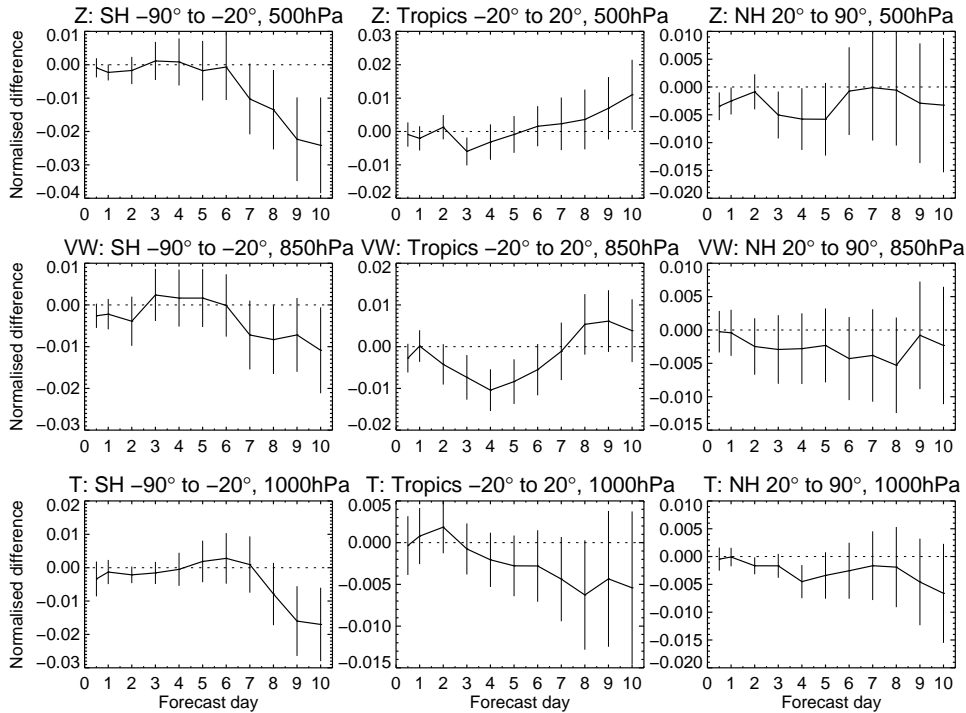


Figure 13: Change in standard deviation of forecast minus analysis as a function of forecast day for experiments testing the new observation errors with no change in screening. Values are shown for top) geopotential height at 500hPa averaged over the Southern Hemisphere, Tropics and Northern Hemisphere (left-to-right), middle) vector wind at 850hPa averaged over the Southern Hemisphere, Tropics and Northern Hemisphere (left-to-right) and bottom) Temperature at 1000 hPa averaged over the Southern Hemisphere, Tropics and Northern Hemisphere (left-to-right). Error bars indicate statistical significance in the 95th percentile and values below zero indicate a reduction in the standard deviation of forecast minus analysis.

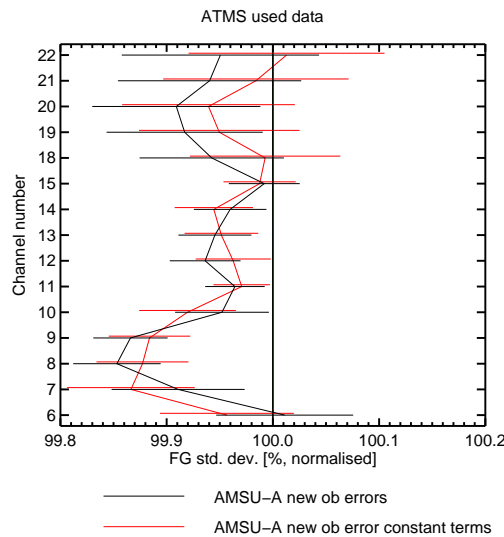


Figure 14: Normalised change in standard deviation of observation minus background (12-hour forecast) for the ATMS instrument, as a function of channel number. Values are for used data, averaged globally, and are shown for the Emissivity forward model error experiment and Satellite-dependent observation error experiment.

found to be small, with a less than 0.01 K change for the different AMSU-A instruments (results not shown).

7.2 Assimilation Trials for relaxed screening

7.2.1 Land and Sea-ice

A number of assimilation trials were run to further test the emissivity observation error terms by relaxing some of the quality control checks and assimilating more AMSU-A data over land and sea-ice. The following trials were run:

- Control: Full ECMWF observing system with current AMSU-A observation errors and screening.
- Global orography: Channels 5 - 6 orography screening replaced by an observation error screen where channel 5 data with $\sigma_{emis} > 0.25$ K are rejected and channel 6 data with $\sigma_{emis} > 0.20$ K are rejected, over land.
- Southern Hemisphere sea-ice: Channel 5 data are added over the Southern Hemisphere sea-ice (and no change to the orography screening).
- Orography excluding Antarctica: Channels 5 - 6 orography screening replaced by an observation error screen, as for the ‘Global orography’ experiment, everywhere excluding Antarctica.

Assimilation trials were run for ECMWF cycle 40R1 at a horizontal resolution of T511. For these tests the AMSU-A observation errors included the forward model terms but not the new satellite-dependent constant terms, i.e. observation errors of:

$$\sigma_o^2 = \sigma_{lwp}^2 + \sigma_{emis}^2 + \sigma_{constant}^2, \quad (15)$$

with constant terms $\sigma_{constant} = 0.25$ K for channel 5 and $\sigma_{constant} = 0.20$ K for channels 6 - 8, which is the same as the operationally applied observation errors for channels 6 - 8 and slightly lower for channel 5 (0.25 K instead of 0.28 K). Operational observation errors were used for other channels. This combination of observation errors was tested previously without screening changes (Lawrence and Bormann, 2014) and found to have a neutral impact. Trials were run for 15 June - 7 August 2013, a period of almost 3 months in the Southern Hemisphere winter (in order to test the impact during a period of Southern Hemisphere sea-ice).

Results of these trials are summarised in Fig. 15, which shows an example of forecast scores of temperature at 500hPa over the Southern hemisphere (a) and the change in short-range forecast fits to ATMS observations (b). The assimilation trial adding data over orography with the exclusion of Antarctica led to a neutral impact on forecast scores of vector wind, temperature, humidity and geopotential. Adding data over Antarctica led to a negative impact in the Southern Hemisphere for the short-range forecast scores (days 1 - 3), however. This negative impact can be seen more clearly in latitude-pressure plots, as shown in Fig. 16(a and b). Note that the apparent positive impact below 700hPa in these plots is misleading because this is in areas of very high orography over Antarctica, where the surface is higher than 700hPa (but below 500 hPa). A negative impact was also observed in the ATMS background departures (used data), when adding data over Antarctica, as shown in Fig. 15b. This indicates a degradation in the short-range forecasts over the Southern Hemisphere ocean, since ATMS data is not used over Antarctica or sea-ice.

Adding channel 5 over sea-ice did not result in a negative impact on the short-range forecasts and even shows a small positive impact on day 2 temperature forecasts for latitudes below 60°S, as shown in Fig. 16b. However,

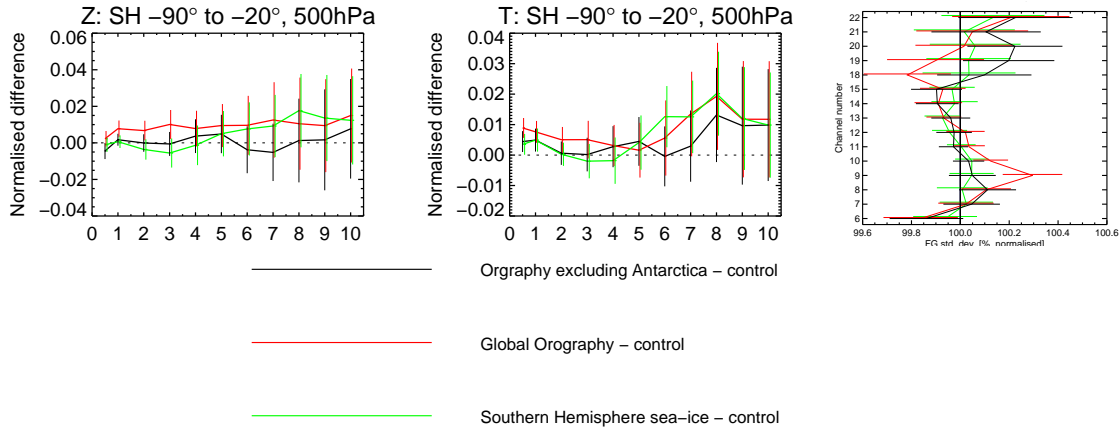


Figure 15: a) Change in the standard deviation of geopotential forecast minus own analysis at 500hPa over the Southern Hemisphere, as a function of forecast day and b) as a) but for temperature, and c) Change in the standard deviation of observation minus background for ATMS over the Southern Hemisphere for the different experiments normalised by the control values.

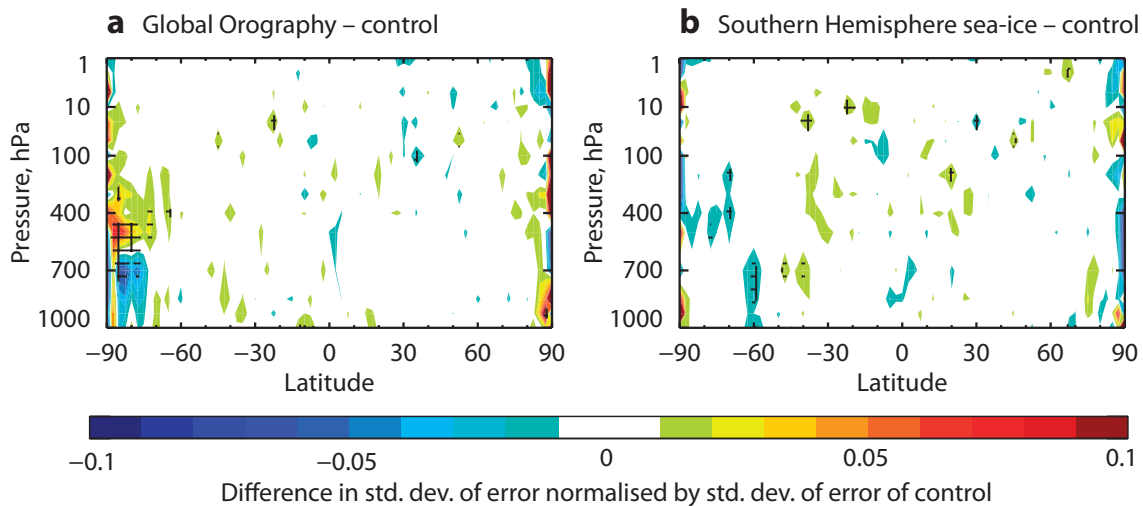


Figure 16: Change in the standard deviation of 3-day temperature forecast minus (own) analysis for the experiment minus the control, plotted as a function of latitude and pressure for the day 2 forecast. Values are for a) ‘orography’ minus control and b) ‘sea-ice’ minus control

a negative impact can be seen at longer ranges (days 6 - 8). It is a little surprising to see this longer-range impact, when there is no negative impact at shorter ranges. There is a possibility that it is simply random, and would disappear for an experiment run over a longer period. However it could also be a real signal, due to the change in the introduction of data over sea-ice. There is also a change in the mean analysis temperature, shown in Fig. 17b over sea-ice, which is likely to be due to adding locally-biased data. This could have a detrimental impact since Data Assimilation theory assumes unbiased background and observations and adding data which is biased relative to the model background could create problems for the assimilation.

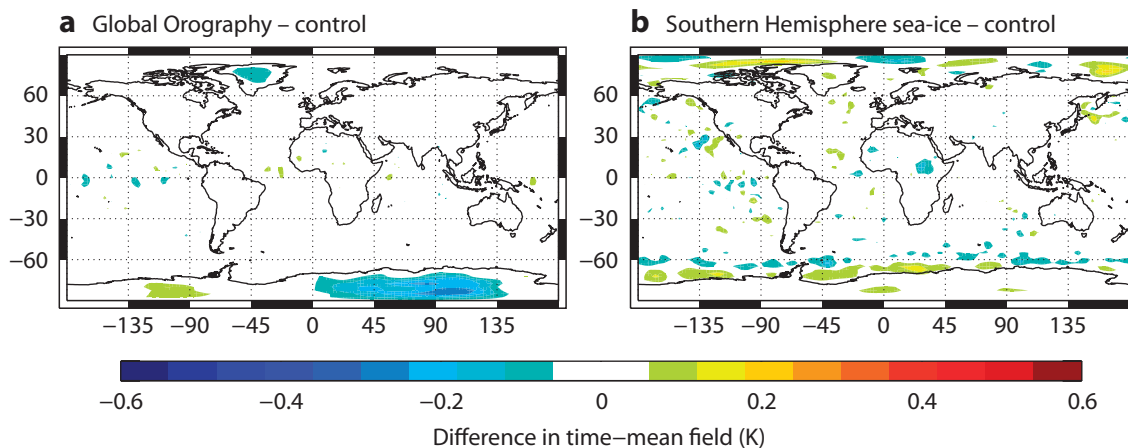


Figure 17: Map of the change in mean temperature analysis at 0h (left) for a) ‘orography minus control at 500hPa, and b) ‘sea-ice minus control at 850 hPa.

Changes in the mean analysis temperature were observed when adding data over Antarctica, the Southern Hemisphere sea-ice and Greenland, as shown in Fig. 17. These changes are likely to be due to adding AMSU-A data which is biased with respect to the background. The mean (bias-corrected) background departures of AMSU-A channel 5 (used data) were approximately 0.2 K over sea-ice and channels 5 and 6 had biases of approximately -0.2 K for used data over Antarctica. The changes in mean analysis over the Southern Hemisphere were accompanied by a degradation in forecast scores, whereas the change in mean analysis temperature over Greenland did not lead to a degradation in forecast scores, as shown in Fig. 15a.

The results of these trials led to the change in orography screening excluding Antarctica being selected for the contribution to 41R2, i.e. the screening change for the ‘Orography excluding Antarctica’ experiment. This change in screening showed a neutral impact on forecast scores, whereas all other tested changes in orography and sea-ice screening showed some negative impacts. Using more data and obtaining a neutral impact is still good, since adding data to the assimilation system makes it more robust, even if it does not noticeably improve forecast scores. If we lose other data in these areas, either for a short time or permanently, the new AMSU-A data could become important.

7.2.2 Ocean cloud screening

Assimilation trials were run both to test the cloud liquid water path error term by adding new data with higher observation errors, and to test whether the operational cloud screening could be relaxed to allow the assimilation of more data. In order to do this we remove the window channel background departure check over ocean for channels 5 - 8 and replace it with a scattering index check, as described in section 3.3. The current liquid water path check is retained. Since there are higher biases for channel 5 data, we decided to also test the change in

cloud screening for channels 6 - 8 only, as well as for channels 5 -8. Results of both sets of trials are presented here. The following three assimilation trials were run (each for summer and winter periods):

- Control: ECMWF cycle 41R1 with no changes to AMSU-A observation errors or screening,
- ‘ $SI < 5$ K screen ch 5 - 8’: The new liquid water path observation errors, with the background departure cloud-check over ocean removed for channels 5 - 8 and replaced by a new scattering index check, removing data with $SI > 5$ K for channels 5 -7 globally and channel 8 over the Tropics,
- ‘ $SI < 5$ K screen ch 6 - 8’: As ‘ $SI < 5$ K screen ch 5 - 8’ but with the cloud screen changed only for channels 6 - 8, excluding channel 5.

The observation errors used for these tests included the cloud liquid water path terms over ocean for channels 5 - 7, without the emissivity error terms or the new satellite-dependent constant terms. The observation errors were thus calculated as follows over ocean:

$$\sigma_o^2 = \sigma_{lwp}^2 + \sigma_{constant}^2. \quad (16)$$

Over land and sea-ice and for channels 8 - 13 the operational observation errors were used. Constant values of $\sigma_{constant} = 0.27$ K were chosen for channel 5 over ocean, and $\sigma_{constant} = 0.20$ K for channels 6 - 7, which were chosen so that the average observation error before the screening change was the same as the control (to within 2 decimal places). This observation error set-up was previously tested with no change in cloud screening and results (not shown) indicated a neutral impact. All assimilation trials were run at a horizontal resolution of T639 with cycle 41R1 of the ECMWF model, and with 137 levels in the vertical. The trials were run over 2 separate periods of 3 months each, covering 1 February - 30 April 2014 and 1 June - 31 August 2014.

Generally, a neutral impact on forecast scores was observed both for the ‘ $SI < 5$ K screen ch 5 - 8’ and for the ‘ $SI < 5$ K screen ch 6 - 8’ experiments, as shown by Fig. 18. The background fits to other observations showed some improvements for the ATMS instrument, however, as shown in Fig. 19. The fit to ATMS is a good indication of improvements in the short-range forecast (due to an improved analysis), since it is essentially an AMSU-A instrument and so has sensitivities to the same heights of the atmosphere as AMSU-A, but the cloud-screening and observation errors have not been changed. Fig. 19 shows a larger improvement for the ‘ $SI < 5$ K screen ch 5 - 8’ experiment than for the ‘ $SI < 5$ K screen ch 6 - 8’ experiment, with an improvement in the fits to ATMS channel 6 (equivalent to AMSU-A channel 5) in both hemispheres and channel 7 (equivalent to ATMS channel 6) in the Northern Hemisphere. The ‘ $SI < 5$ K screen ch 6 - 8’ experiment does not show the improvement for ATMS channel 6, but it does show the improvement for channel 7, which is likely due to the additional AMSU-A channel 6 data.

Although the fits to ATMS indicate a general improvement when adding more channel 5 data, there are however some local degradations in the short-range forecasts over the Southern Hemisphere ocean for the February - April period which can be observed when looking in more detail at maps of forecast scores, as shown in Fig. 20(a) for the 12-hour 1000hPa temperature forecast scores. This was also seen for cycle 40R1 (presented previously by Lawrence and Bormann (2014)), and this degradation is seen for both the 12-hour and 24-hour forecasts minus analyses. It is accompanied by a change in mean analysis over this period, also shown in Fig. 20(c). Given that this is in an area of liquid water cloud and that the mean change is to increase temperature, both these effects could be due to the assimilation system aliasing cloud effects into temperature increments. Over the June - August period a similar degradation is not seen, which is possibly due to the shift in areas of high liquid water path in different seasons. Over the Southern Hemisphere there are fewer conventional observations, so this aliasing is more likely to happen over the Southern Hemisphere. Even though forecast

scores and fits to background show some improvement in overall forecast accuracy when assimilating the new data for channels 5 - 8, this negative impact in certain local areas is nevertheless something that we wish to avoid. When changing the cloud screening for only channels 6 - 8 the local Southern Hemisphere degradation is no longer observed, as shown in Fig. 20(b) and the change in mean analysis is also not observed, as shown in Fig. 20(d). This indicates that the degradation does indeed come from the channel 5 data. Additional trials were run combining a window channel background departure check with thresholds of 5 K and 10 K (higher than the thresholds used operationally) for channel 5, along with the new cloud screening for channels 5 - 8. These trials were found to reduce the negative impacts due to channel 5, shown in Fig. 20, but not completely remove it (results not shown).

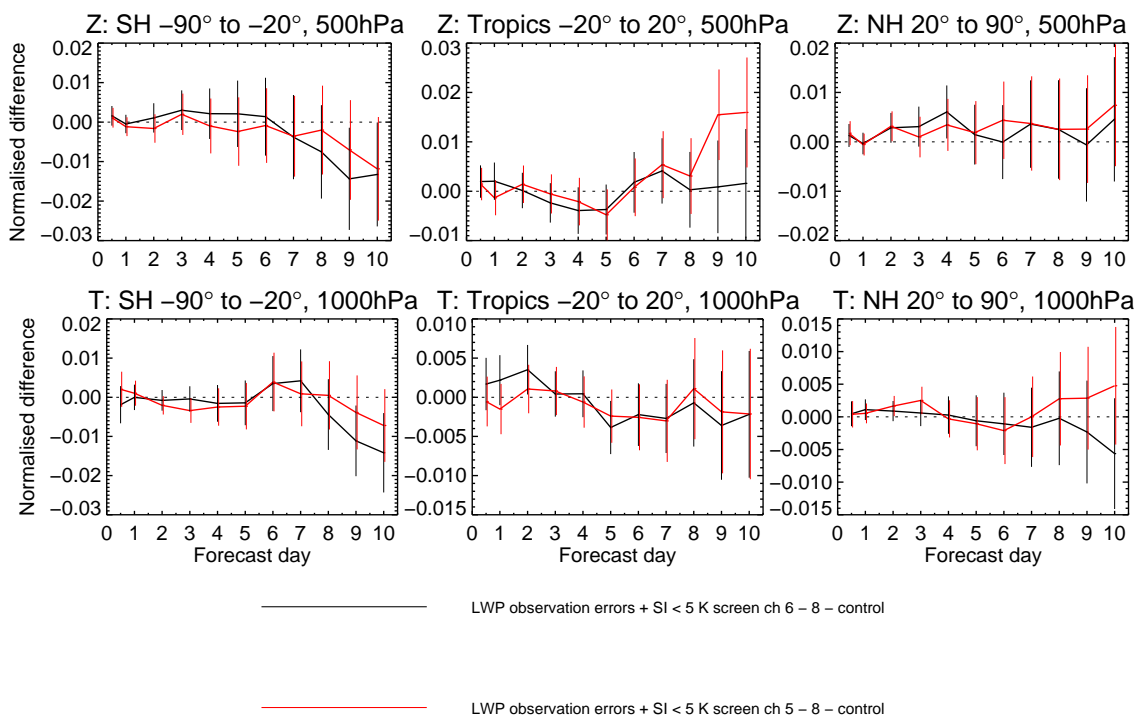


Figure 18: Change in standard deviation of geopotential forecast minus own analysis at 500 hPa (top) and temperature forecast minus own analysis at 1000hPa (bottom) for both the ‘SI < 5 K screen ch 5 - 8’ and ‘SI < 5 K screen ch 6 - 8’ experiments combining both periods (1 February - 30 April 2014 and 1 June - 30 August 2014).

Results presented in this section led us to select the change in cloud screening for channels 6 - 8 for the contribution to cycle 41R2, and to keep the current cloud screening for channel 5 (of a background departure check with a liquid water path check). Although there is some evidence that the change in screening for channel 5 has a positive overall impact (improvements in fits to ATMS) there is also some evidence of localised degradations over the Southern Hemisphere ocean, which led us to not include the change of screening of channel 5 in the contribution to cycle 41R2.

8 New AMSU-A observation errors + screening changes: combined contribution to 41R2

Following the results of assimilation trials testing the new observation errors and different changes in the screening, a combination of new observation errors with a change in orography and cloud-screening was selected as

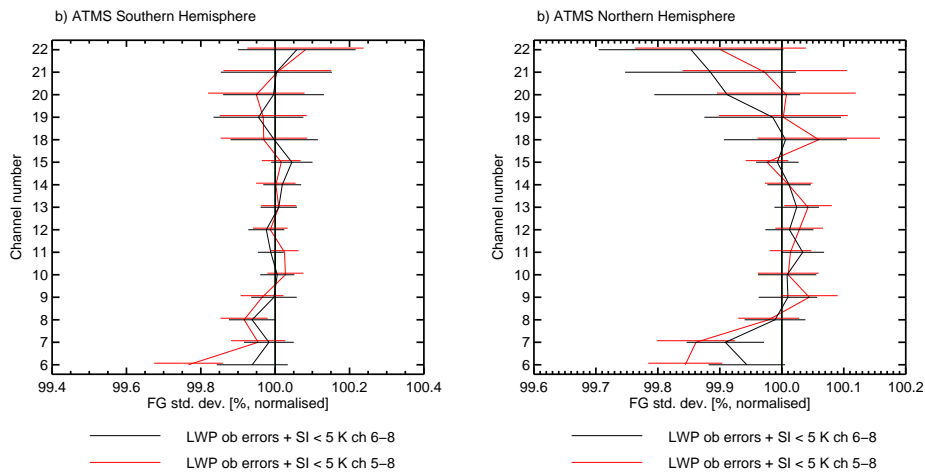


Figure 19: Standard deviation of background departures for ATMS for the ‘LWP observation errors + SI < 5 K screen ch 5 - 8’ and ‘LWP observation errors + SI < 5 K screen ch 6 - 8’ experiments normalised by the control, averaged over a) the Southern Hemisphere extra-tropics and b) the Northern Hemisphere extra-Tropics.

a contribution to cycle 41R2 of the ECMWF model. This contribution included:

- New AMSU-A Satellite-dependent observation errors for channels 5 - 13 ($\sigma_{constant}$) and emissivity and cloud liquid water observation error terms for channels 5 - 8 (σ_{emis} and σ_{lwp} respectively). These new observation errors can be calculated from (12) - (13).
- Replacing the orography screening over land, excluding Antarctica, with an observation error check which rejects data with $\sigma_{emis} > 0.25$ K for channel 5, $\sigma_{emis} > 0.20$ K for channel 6.
- Replacing the window channel background departure check over ocean for channels 6 - 8 with a Scattering Index (SI) check rejecting data with $SI > 5$ K

As a result of the changes in screening, new AMSU-A data were added for channels 5 - 8 by approximately 6 % for channel 5, 12 % for channel 6, 9 % for channel 7 and 3 % for channel 8. This is shown in Fig. 21.

The new observation errors combined with new screening changes were tested in a series of assimilation trials over 2 periods of 3 months for 1 February - 30 April 2014 and 1 June - 31 August 2014. Results of these indicate a small improvement in forecast scores over the Northern Hemisphere and neutral impact over the Tropics and Southern Hemisphere, as demonstrated in Fig. 22. There was also a reduction in the standard deviation of background departures for ATMS, as shown in Fig. 23, which indicates an improvement in short-range forecasts.

9 Conclusions

New observation errors were developed for AMSU-A, which included constant terms for channels 5 - 13, and forward model errors due to emissivity uncertainty for channels 5 - 8 and cloud effects for channels 5 - 7. The new constant terms were different for each channel of each satellite, in order to reflect the different instrument noise for each satellite and channel. The global averages of observation errors for each channel were kept to be the same (with only a small increase of 0.02 K for channel 5) so that the main effect was to re-weight the data depending on satellite and atmospheric and surface conditions.

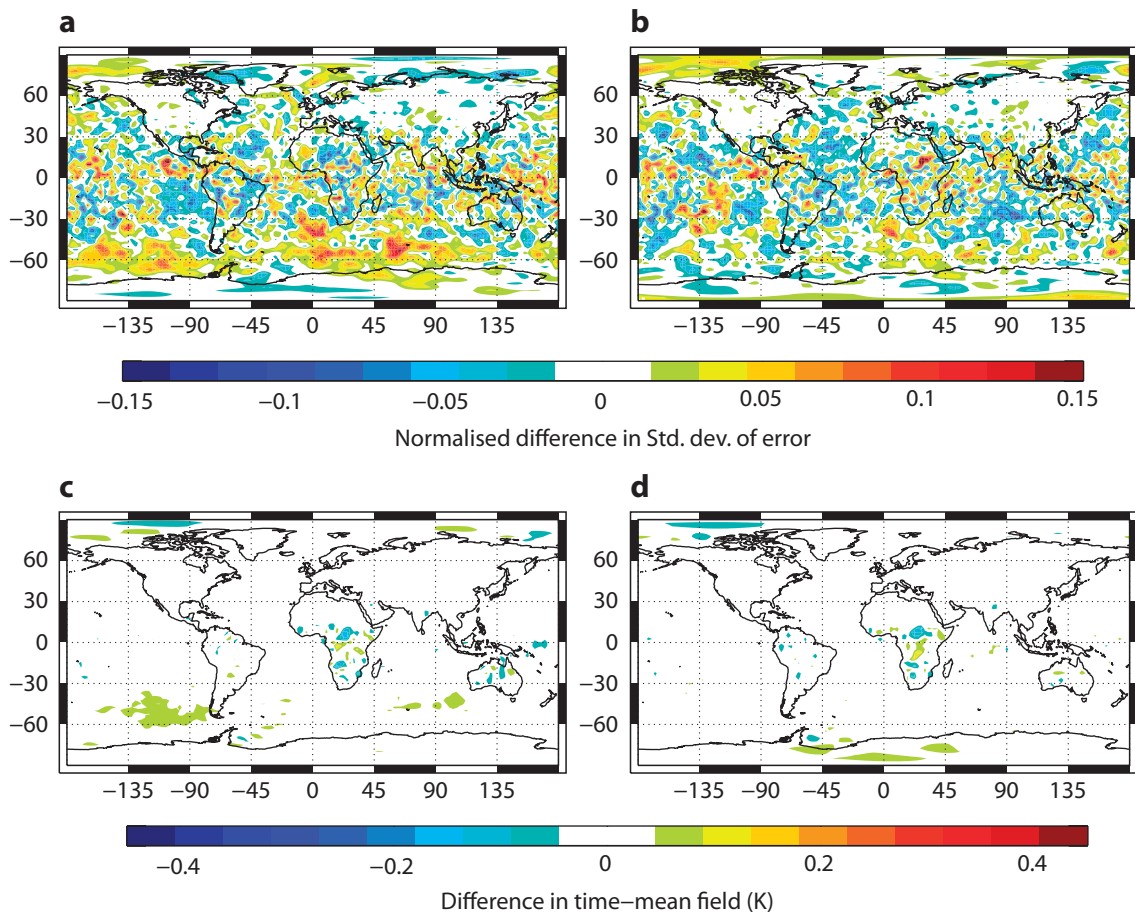


Figure 20: a) Change in standard deviation of 1000hPa 12-hour temperature forecast minus own analysis between the 'LWP observation errors + SI < 5 K screen ch 5 - 8' screen experiment and control for the 1 February - 30 April 2014 period, b) same as a) but for the 'LWP observation errors + SI < 5 K screen ch 6 - 8', c) Change in the mean temperature analysis at 1000hPa for the 'LWP observation errors + SI < 5 K screen ch 5 - 8' experiment minus control for the 1 February - 30 April 2014 period, d) same as c) but for the 'LWP observation errors + SI < 5 K screen ch 6 - 8' experiment minus control

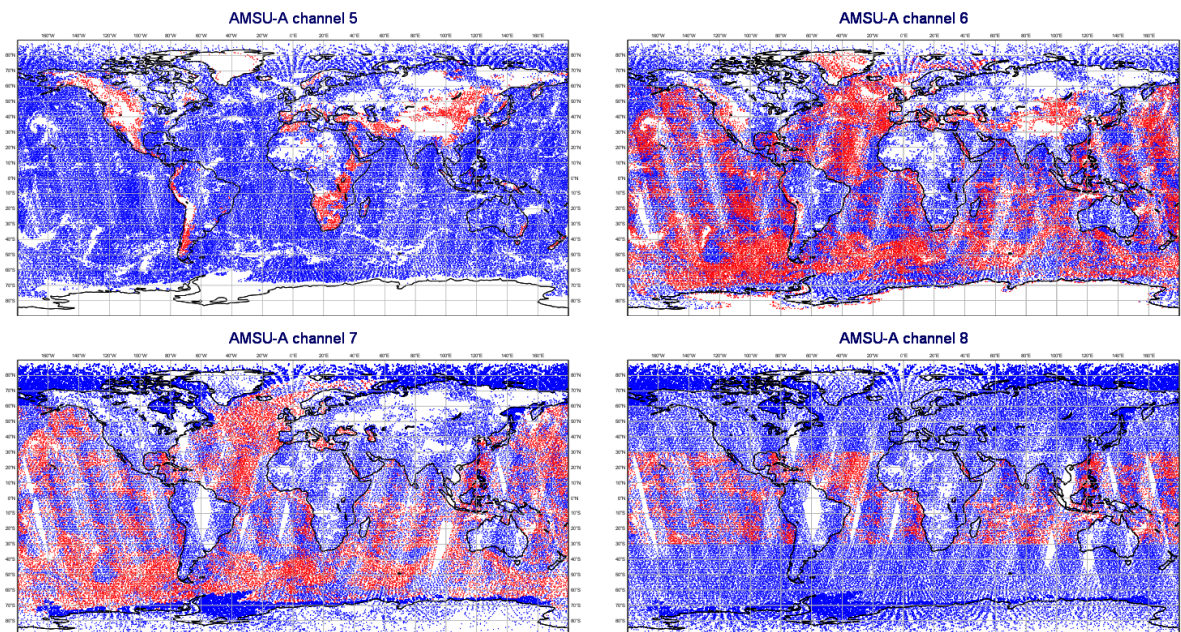


Figure 21: Geographic coverage of AMSU-A data assimilated for one cycle of the ECMWF NWP model on 1 February 2014, channels 5 - 7, with the new AMSU-A observation errors and screening for cycle 41R2. Areas shown in red indicate the new data and blue indicate the data used previously as well.

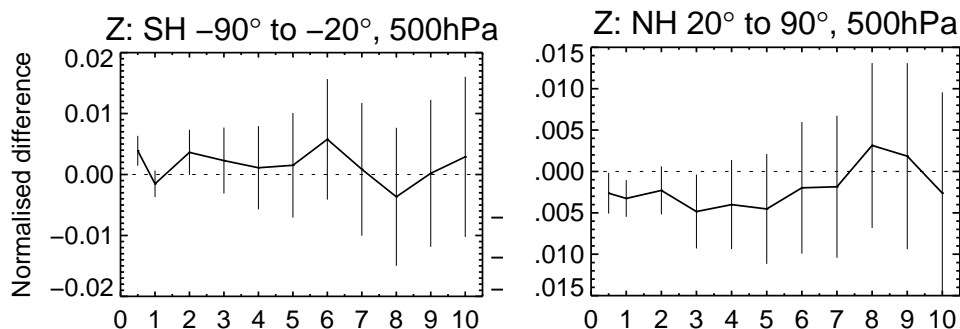


Figure 22: Change in standard deviation of vector wind forecast minus analysis at 500hPa for the contribution to 41R2 experiment minus the control, over a) the Southern Hemisphere extra-Tropics, and b) the Northern Hemisphere extra-Tropics

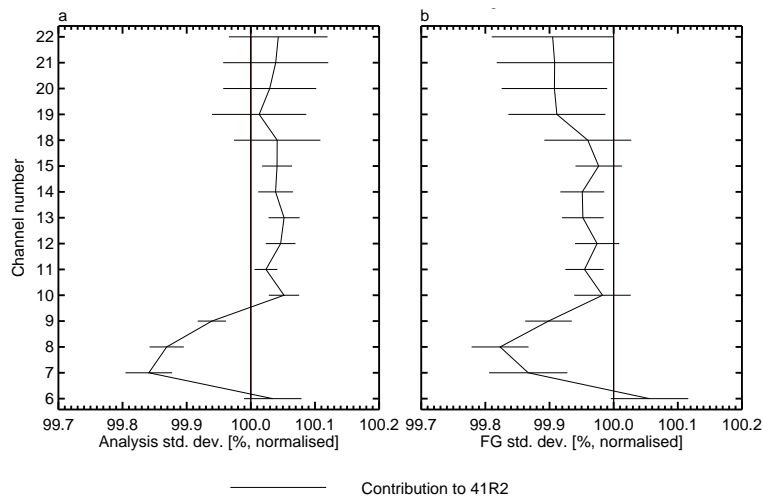


Figure 23: Normalised change in standard deviation of a) observation minus analysis and b) observation minus background (12-hour forecast) for the ATMS instrument, as a function of channel number. Values are for used data, averaged globally.

The new observation errors were tested in assimilation trials firstly without changing the operational cloud, orography and sea-ice screening. Secondly different ways of changing the screening were tried, which allowed more data to be assimilated. Results showed:

- The new observation errors led to an improvement in the fit of short-range forecasts to the ATMS instrument, of up to 0.1%, which was found to be due to the new satellite-dependent constant terms.
- Relaxing the orography screening on top of the new observation errors, with the exclusion of Antarctica, led to a neutral impact on forecast scores.
- Relaxing the orography screening over Antarctica and the sea-ice screening over the South Pole led to some negative impacts on forecast scores, ATMS background departures and a change in the mean analysis in these regions, thought to be due to introducing biased data.
- Changing the cloud screening for channels 5 - 8 on top of the new observation errors led to an improvement in the background departures of ATMS (0.1 - 0.2%) and a generally neutral impact on forecast scores with the exception of a negative impact for 12-hour - 1 day 1000hPa temperature forecasts in areas of Southern Hemisphere liquid cloud. This negative impact was found to be due to the introduction of channel 5 data in these areas.
- Changing the cloud screening for channels 6 - 8 led to a neutral impact on forecast scores, and improved the background departures of ATMS channel 7 by up to 0.1 %.

On the whole there is evidence of an improvement in short-range forecast accuracy when using the new satellite-dependent noise terms, and the new cloud forward model errors with a change in cloud screening for channels 6 - 8. Adding biased data, however, generally led to a degradation over the Southern Hemisphere, particularly when adding data over Antarctica or relaxing the cloud screening for channel 5 in the Southern Hemisphere.

As a result of these assimilation trials a combination of the new observation errors with screening changes which gave the best results was selected and tested. This included relaxing the cloud screening for channels 6 - 8 and the orography screening for channels 5 - 6, with the exception of over Antarctica. Results of these tests

led to a small positive impact in forecast scores over the Northern Hemisphere (up to 0.5 % for days 1 - 3) and an improvement in the short-range forecast fits to ATMS observations of 0.05 - 0.2 % for channels 7 - 14. This combination of new observation errors and change in screening was included in cycle 41R2 of the ECMWF Integrated Forecasting System (IFS) model.

Acknowledgements

Heather Lawrence's work at ECMWF is funded by the EUMETSAT fellowship programme.

References

- E Andersson and H Jarvinen. Variational quality control. *ECMWF Technical Memorandum*, 250, 1998.
- T. Auligné, A. McNally, and D.P. Dee. Adaptive bias correction for satellite data in a Numerical Weather Prediction system. *Q. J. R. Meteorol. Soc.*, 133:631–642, 2007.
- N. Bormann and P. Bauer. Estimates of spatial and inter-channel observation error characteristics for current sounder radiances for NWP, part I: Methods and application to ATOVS data. *Q. J. R. Meteorol. Soc.*, 136: 1036–1050, 2010.
- D. Dee. Variational bias correction of radiance data in the ECMWF system. *Proceedings ECMWF Workshop on Assimilation of high spectral resolution sounders in NWP, 28 June - 1 July 2004*, 2004.
- G. Desroziers, L. Berre, B. Chapnik, and P. Poli. Diagnosis of observation, background and analysis-error statistics in observation space. *Q. J. R. Meteorol. Soc.*, 131:3385–3396, 2005.
- E. Di Tomaso and N. Bormann. Assimilation of ATOVS radiances at ECMWF: first year EUMETSAT fellowship report. *EUMETSAT/ECMWF Fellowship Programme Research Report*, 22, 2011.
- E. Di Tomaso and N. Bormann. Assimilation of ATOVS radiances at ECMWF: third year EUMETSAT fellowship report. *EUMETSAT/ECMWF Fellowship Programme Research Report*, 29, 2013.
- S.J. English. The importance of accurate skin temperature in assimilating radiances from satellite sounding instruments. *IEEE Trans. Geoscience. Rem. Sensing.*, 46:403 – 408, 2008.
- S.J. English and T.J. Hewison. A fast generic microwave emissivity model. In *T. Hayasaka, D.L. Wu, Y. Jin, and J. Jiang (Eds.), Proceedings of SPIE, 3503*, pages 288 – 300, 1998.
- A. Geer and P. Bauer. Observation errors in all-sky data assimilation. *Q. J. R. Meteorol. Soc.*, 137:2024–2037, 2011.
- A. Geer, P. Bauer, and S. English. Assimilating AMSU-A temperature sounding channels in the presence of cloud and precipitation. *ECMWF Tech. Memo.*, 670, 2012.
- F. Karbou, E. Grard, and F. Rabier. Microwave land emissivity and skin temperature for amsu-a and -b assimilation over land. *Q.J.Roy.Met.Soc.*, 132:2333–2355, 2006.
- M. Kazumori and S. English. Use of the ocean surface wind direction signal in microwave radiance assimilation. *Quart. J. Roy. Meteorol. Soc.*, in press, 2014.

- H. Lawrence and N. Bormann. First year report: The impact of HIRS on ECMWF forecasts, adding ATMS data over land and sea-ice and new observation errors for AMSU-A. *EUMETSAT/ECMWF Fellowship Programme Research Report*, 34, 2014.
- Q. Liu, F. Weng, and S. English. An improved fast microwave water emissivity model. *IEEE Trans. Geosci. Remote Sens.*, 49:1238 – 1250, 2011.
- K. Salonen, J. Cotton, N. Bormann, and M. Forsythe. Characterizing AMV height-assignment error by comparing best-fit pressure statistics from the Met Office and ECMWF data assimilation systems. *Journal of Applied Meteorology and Climatology*, 54:225 – 242, 2015.
- P. Watts and A. P. McNally. Identification and correction of radiative transfer modelling errors for atmospheric sounders: AIRS and AMSU-A. *Proceedings of the ECMWF Workshop on Assimilation of High Spectral Resolution Sounders in NWP*, ECMWF, Reading, UK., 2004.